Glucose-dependent signalling pathways regulate TE differentiation in bovine embryos

Jinlong Qiu[1] and Roger Sturmey[1]

1. Centre for Biomedicine, Hull York Medical School, University of Hull, Hull, HU6 7RX, UK

Abstract

Glucose uptake and metabolism increase markedly during the transition from morula to blastocyst. However, the functional roles of glucose during this process in bovine embryos remain incompletely understood. Here, we demonstrate that glucose specifically modulates trophectoderm (TE) differentiation without affecting the inner cell mass (ICM), acting through Hippo signalling via the hexosamine biosynthetic pathway (HBP) and the pentose phosphate pathway (PPP) rather than glycolysis. Consistently, scRNA-seq analysis reveals that unlike glycolysis-related genes, which show only stage-specific changes, HBP- and PPP-related genes exhibit significant differential expression between the TE and ICM lineages. Furthermore, we found that glucose deprivation does not impair pyruvate uptake or intracellular pyruvate levels in blastocysts, yet it significantly depletes the terminal metabolites of the HBP and PPP. Together, these findings reveal that glucose-dependent regulation of TE differentiation is conserved in bovine embryos.

Introduction

Glucose is a key metabolic substrate during early embryonic development [1, 2]. Classical models of glucose metabolism presumed that glucose is predominantly catabolized through glycolysis to generate pyruvate, which enters the tricarboxylic acid (TCA) cycle to satisfy the energetic requirements of cell proliferation and development [3, 4].

However, recent studies in mouse embryos have challenged this traditional bioenergetic view of glucose metabolism [5-7]. These studies demonstrate that, during early preimplantation development, glucose contributes only minimally to glycolytic

flux and ATP production [5-7]. Instead, glucose-derived carbon is preferentially channeled into HBP and PPP, supporting biosynthetic processes and redox homeostasis [5, 7].

In particular, HBP-derived O-linked N-acetylglucosaminylation (O-GlcNAc) has been implicated in the regulation of the Hippo signaling pathway, thereby influencing TE-associated transcriptional programs [5, 8, 9]. In parallel, the PPP has been shown to function upstream of mechanistic target of rapamycin (mTOR) signaling to regulate TE specification [5, 10, 11]. Whether this glucose-driven signaling paradigm is conserved across bovine embryogenesis, however, remains to be elucidated.

In this study, we demonstrate that while glucose-mediated regulation of the TE program is conserved in bovine embryos, their metabolic dependency is significantly more intricate than that observed in murine models. Notably, bovine embryos exhibit a heightened tolerance to glucose deprivation, retaining the capacity for blastocyst formation even in its absence. Furthermore, the contributions of the HBP and PPP appear highly context-dependent, with developmental outcomes varying according to the timing of inhibition and the specific metabolic nodes targeted. Collectively, our findings underscore a critical role for glucose in the TE formation of large mammals while revealing the nuanced metabolic architecture underlying this process.

Materials and methods

Unless specified otherwise, all reagents and chemicals were obtained from Merck (Dorset, UK).

In vitro bovine embryo production

In vitro maturation (IVM), fertilization (IVF), and culture (IVC) of bovine embryos were performed according to previously described protocols with minor modifications [12-14]. IVM, IVF, and SemenPrep media were obtained from IVF Bioscience (Falmouth, UK). Bovine ovaries were harvested from animals slaughtered for commercial purposes unrelated to the study. Ovaries were collected and transported to the laboratory within 2 hours of slaughter. Cumulus–oocyte complexes (COCs) were collected from 3–8 mm follicles on the ovarian surface. COCs were cultured in IVM medium at 39°C, 5% CO_2 for

22 hours. Following maturation, groups of 25–30 COCs were co-incubated with spermatozoa (Genus Plc) (1–5 × 10^6/mL) purified from frozen–thawed semen using SemenPrep medium. IVF was carried out at 39°C, 5% CO_2 for 10–14 hours. After fertilization, cumulus cells were removed. Presumptive zygotes were subsequently cultured in BO-SOF medium supplemented with either 0 mM or 1.5 mM glucose at 39 °C, 5% CO_2 and 5% O_2.

The BO-SOF formulation was prepared according to the protocol described in our previous publication [15, 16]. The inhibitors used in this study are listed in Supplementary Table 1. Unless otherwise stated, inhibitors were dissolved in BO-SOF and added from E0. The inhibitor concentrations were selected based on previously published studies [5, 17].

Metabolic assay

Morula-stage embryos were individually cultured for 24 hours in 5-µL microdrops, after which embryos that successfully developed to the blastocyst stage were identified and their spent culture media were collected. All samples were immediately stored at −78°C until subsequent metabolic assays. Pyruvate concentrations were quantified using enzyme-coupled fluorometric methods adapted from a previously established protocol [15]. All enzymes used for metabolic analyses were obtained from Roche (Burgess Hill, UK). Standard curves were generated from serial dilutions of freshly prepared metabolite standards. Fluorescence values were calculated as the difference between pre- and post-incubation readings and converted to absolute concentrations. All measurements were performed in technical triplicate, and assays with standard curve R^2 values < 0.98 were excluded from further analysis.

Measurement of Basal Oxygen Consumption Rate (OCR)

The OCR detection protocol is based on previously published articles [16]. Briefly, OCR was assessed using a Seahorse XFp Analyzer (Agilent Technologies). Seahorse analysis was performed following the manufacturer's recommendations for OCR. Embryos were allocated in small groups (6-10 bovine blastocysts per well) in 180 µl of HEPES-buffered SOF medium appropriate for the developmental stage.

87 **JC-1 staining**

88 JC-1 (Thermo Fisher) was initially dissolved in DMSO and subsequently diluted to a final
89 concentration of 1 μM in SOF medium. Embryos were incubated in this solution for
90 30 minutes under standard culture conditions. Following three washes with HEPES-
91 buffered SOF, the embryos were imaged using a Zeiss LSM710 confocal microscope.

92 **Immunofluorescence (IF)**

93 Samples were first washed three times with 0.1% polyvinylpyrrolidone/phosphate-
94 buffered saline (PBS), then fixed with 4% paraformaldehyde/PBS for 30 minutes and
95 then permeabilized with 0.5% Triton X-100/PBS for 30 minutes at room temperature. The
96 blocking step was performed in blocking buffer (PBS containing 10% FBS and 0.1%
97 Triton X-100) for 1 hour. Afterwards, samples were incubated overnight with primary
98 antibodies in blocking buffer at 4°C. After three washes, embryos were incubated with
99 secondary antibodies for 2 hours. Finally, samples were stained with Hoechst3342
100 (Hoechst) (Merck) for 15 minutes and then mounted. Images were acquired using
101 inverted fluorescence microscope (Zeiss AXIO Vert.A1) or a laser scanning confocal
102 microscope (Zeiss LSM 710) with a 40x objective lens.

103 FIJI (https://imagej.net/software/fiji/) was used for image visualization, cell counting,
104 and signal intensity measurements. Depending on the experiment, signal intensity was
105 measured and background subtracted to analyze absolute intensity. All antibodies
106 (Supplementary Table S2 and S3) were validated to react with bovine cells [12, 18, 19].

107 **Single-cell RNA-seq data acquisition and processing**

108 The single-cell RNA sequencing dataset of bovine preimplantation embryos analyzed in
109 this study was obtained from the publicly available Gene Expression Omnibus (GEO)
110 database under accession number GSE239782 [20]. This dataset contains
111 transcriptomic profiles of bovine embryos at defined developmental stages, including
112 morula, early blastocyst, mid-blastocyst, and late blastocyst stages. Raw count
113 matrices were downloaded and processed using the Seurat R package (version 4.5.2).
114 The calculation of module scores and all analysis codes were adapted from previously
115 published studies [21].

116 **Statistical Analysis**

117 Unless otherwise noted, all experiments were performed with at least three biological
118 replicates. Differences between groups were evaluated using two-tailed unpaired
119 Student's t-tests. Graphs were generated with GraphPad Prism 10.

120 Results

121 **Glucose plays a role in blastocyst formation**

122 To investigate the functional requirement for glucose during bovine preimplantation
123 development, embryos were cultured from embryonic day 0 (E0) in either glucose-free
124 medium (G−) or control medium (CTRL). Subsequent monitoring revealed no significant
125 differences in developmental rates between the G− and CTRL groups at the 4-cell
126 (E2.0), 8–16-cell (E3.5), or morula (E5.0) stages (Fig. 1A, B). However, by E6.5, blastocyst
127 formation rates were markedly reduced in the G− group (Fig. 1A, B). Furthermore, those
128 few embryos that successfully reached the blastocyst stage failed to hatch normally by
129 E8.5 (Fig. 1C, D). This morphological impairment was accompanied by a significant
130 reduction in total cell count, a deficit that was already detectable as early as the morula
131 stage (Fig. S1A–D). Collectively, these data suggest that while glucose is not strictly
132 required for the blastocyst transition, it is indispensable for achieving optimal
133 developmental efficiency, cellular proliferation, and subsequent hatching. Inhibition of
134 glucose metabolism using the hexokinase inhibitor 2-deoxy-D-glucose (2-DG) similarly
135 reduced blastocyst rate, confirming the important role of glucose in blastocyst
136 formation (Fig. S1F, G).

137 To dissect the contributions of different glucose metabolic pathways, specific inhibitors
138 were used to block glycolysis, HBP, and PPP (Fig. S1E). Inhibiting glucose flux into
139 pyruvate with YZ9 had no effect on blastocyst formation rate (Fig. 1E, F). In contrast,
140 blocking the PPP with 6-aminonicotinamide (6-AN) or the HBP with 6-Diazo-5-oxo-L-
141 norleucine (DON) induced morula-stage developmental arrest (Fig. S1H, J), which could
142 not be rescued by supplementation with their downstream metabolites (Fig. S1I, K).
143 However, inhibition of the downstream HBP enzyme O-GlcNAc transferase (OGT) using
144 ST045849 (TT04) had no effect on blastocyst formation rate (Fig. 1G, H). In addition,
145 when PPP inhibition was delayed until E5.5, embryos were able to reach the blastocyst

146 stage, although the blastocyst formation rate was significantly reduced (Fig. 1I, J).
147 Together, these results demonstrate that glucose supports blastocyst formation through
148 divergent metabolic nodes rather than through a uniform glycolytic requirement.

149 **Glucose metabolism regulates TE through Hippo pathway**

150 To evaluate the impact of glucose on lineage specification, we performed
151 immunofluorescence (IF) analysis on E7.0 blastocysts (Fig. 2A). Quantitative analysis
152 showed that glucose deprivation significantly reduced CDX2 fluorescence intensity and
153 the overall proportion of $CDX2^+$ cells within the blastocyst (Fig. 2B, C). Consistently, the
154 expression of an additional TE marker, GATA3, was also diminished in the absence of
155 glucose (Fig. S2A, B). In contrast, neither the protein levels of the ICM marker SOX2 nor
156 the proportion of $SOX2^+$ cells were significantly altered (Fig. 2B, C). Similarly, the
157 expression and cell count for the epiblast (EPI) marker NANOG and the primitive
158 endoderm (PrE) marker GATA6 remained comparable between groups (Fig. 2D–F). These
159 findings collectively indicate that glucose deprivation selectively impairs TE
160 differentiation while leaving ICM lineage specification largely unaffected.

161 Given the central role of Hippo signalling in TE specification [22, 23], we next examined
162 its activity in response to glucose availability. IF analysis revealed a significant reduction
163 in phosphorylated YAP (p-YAP) levels in G− embryos (Fig. 2I, J). Consistently, the nuclear
164 localization of YAP, as well as the abundance of TE-associated transcription factors
165 TFAP2C and TEAD4, was markedly decreased under G− conditions (Fig. 2G, H, K, L).
166 These results indicate that glucose levels modulate TE program execution via the Hippo-
167 YAP axis. Similar phenotypes were observed following the pharmacological inhibition of
168 glucose metabolism with 2-DG. Treatment with 2-DG significantly reduced total cell
169 counts and shifted the TE-to-ICM ratio in E7.0 blastocysts (Fig. S2E), characterized by a
170 selective suppression of CDX2 while leaving SOX2 levels unaffected (Fig. S2C–F).
171 Furthermore, the expression of YAP, TFAP2C, and p-YAP was significantly diminished
172 following 2-DG treatment (Fig. S2G–J), reinforcing the conclusion that glucose status
173 specifically governs TE differentiation through the regulation of Hippo signaling
174 components.

175 **Glucose availability regulates HBP activity and epigenetic landscapes**

To identify the metabolic drivers of glucose-dependent TE specification, we performed a secondary analysis of publicly available metabolomics data from bovine blastocysts subjected to glucose-free culture [24]. While glucose deprivation led to a broad reduction in intermediates across several metabolic branches, the steady-state levels of pyruvate and ribose were unaffected, indicating that the outputs of glycolysis and the PPP are relatively preserved (Fig. S3A). In contrast, HBP metabolites, including N-acetylglucosamine (GlcNAc) and UDP-GlcNAc, were markedly reduced (Fig. S3A), highlighting a selective vulnerability of the HBP to glucose deprivation.

To validate our metabolomics findings, we first assessed mitochondrial membrane potential (ΔΨm) to assess the impact of glucose availability on cellular energy homeostasis. Glucose deprivation significantly reduced the orange/green JC-1 fluorescence ratio in bovine blastocysts, indicative of mitochondrial depolarization (Fig 3A, B). Interestingly, basal oxygen consumption rates (OCR), measured via Seahorse analysis, remained comparable between G− and CTRL embryos (Fig. 3C). This suggests that while glucose is essential for maintaining ΔΨm, bovine embryos possess the metabolic flexibility to sustain basal respiratory flux through the utilization of alternative substrates [25, 26].

To determine whether embryos compensate for the absence of glucose by increasing reliance on exogenous pyruvate, pyruvate consumption from the culture medium was assessed. Measurement of pyruvate concentrations in spent culture media revealed no significant differences between CTRL and G- embryos (Fig 3D). Consistently, 2-DG or YZ9 inhibition did not significantly alter pyruvate concentration as well (Fig 3E, F). Collectively, these findings indicate that embryos do not trigger a compensatory increase in exogenous pyruvate uptake to offset the energy deficit caused by glucose deprivation.

To validate the impact of glucose withdrawal on the HBP identified in our metabolomics re-analysis, we assessed global O-GlcNAc levels. Consistent with the depletion of HBP intermediates observed in our metabolomics analysis, O-GlcNAc levels were significantly diminished in blastocysts cultured under G− conditions or treated with 2-DG (Fig. 3G, H and Fig. S3C, D). These results verify that restricted glucose availability

206 directly compromises HBP-mediated protein O-GlcNAcylation in the developing
207 embryo.

208 In parallel, our metabolomics re-analysis highlighted significant alterations in
209 metabolites associated with amino acid methylation, specifically those linked to lysine
210 trimethylation (Kme3) and arginine methylation (ADMA and SDMA) (Fig. S3B). Guided by
211 these observations, we examined the relationship between glucose flux and epigenetic
212 remodeling. Both glucose deprivation and 2-DG treatment markedly reduced ADMA and
213 SDMA levels, which was accompanied by a pronounced decrease in the repressive
214 histone mark H3K27me3 (Fig. 3I–N and Fig. S3C–J). These findings establish glucose
215 availability as a key determinant of the epigenetic landscape in bovine blastocysts,
216 likely through the regulation of methyl-donor availability [27].

217 **HBP-Dependent O-GlcNAc Regulates CDX2**

218 To determine whether the HBP signaling axis operates through O-GlcNAc during bovine
219 blastocyst development, we first verified that pharmacological inhibition of OGT (using
220 TT04) significantly reduced global O-GlcNAc levels (Fig. 4G, H). We then assessed the
221 impact of O-GlcNAc inhibition on lineage specification. TT04 treatment specifically
222 downregulated CDX2 expression without perturbing SOX2 levels (Fig. 4A, B), while total
223 cell number and the relative proportions of TE and ICM cells remained unchanged (Fig.
224 4C, D).

225 Given the reduction in CDX2 expression, we next examined the Hippo signaling
226 pathway. TT04-mediated O-GlcNAc inhibition significantly attenuated total YAP protein
227 abundance without altering TFAP2C expression (Fig. 4E, F). Furthermore, TT04
228 treatment triggered a marked increase in phosphorylated YAP (p-YAP) levels (Fig. 4G, H),
229 indicating enhanced YAP phosphorylation and cytoplasmic retention upon O-GlcNAc
230 inhibition. Collectively, these findings demonstrate that O-GlcNAc acts as a critical
231 metabolic signal that preserves TE identity by stabilizing the YAP protein.

232 **PPP–mTOR Signaling Axis Regulates TFAP2C**

233 Glucose-derived nucleotides synthesized via the PPP serve as metabolic signals that
234 activate mTOR signaling [5, 28]. To evaluate mTORC1 activity under glucose deprivation

235 or PPP inhibition, we used phosphorylated ribosomal protein S6 (pS236-RPS6) as a
236 downstream readout. IF analysis revealed a marked reduction in pS236-RPS6 levels in
237 both G− and 6-AN–treated blastocysts compared to CTRL embryos (Fig. 5A–D). These
238 results indicate that PPP-dependent metabolic flux is essential to sustain mTORC1
239 signaling during bovine blastocyst development.

240 Given that mTOR promotes mRNA translation through the phosphorylation of RPS6 [5,
241 10, 11], we next interrogated whether the PPP regulates TFAP2C expression through an
242 mTOR-dependent mechanism. Embryos were treated with the mTOR inhibitor INK128
243 from E0, which effectively suppressed mTORC1 activity, as evidenced by reduced
244 pS236-RPS6 levels (Fig. 5G, H). While mTOR inhibition did not arrest overall blastocyst
245 formation (Fig. 5E, F), it resulted in the significant downregulation of TFAP2C and CDX2
246 protein levels (Fig. 5I, J). Quantitative analysis further demonstrated a reduction in total
247 blastocyst cell numbers following INK128 treatment, which was driven primarily by a
248 selective loss of TE ($CDX2^{+}$) cells, whereas the ICM ($CDX2^{-}$) population remained
249 unaffected (Fig. 5I, K). Collectively, these findings identify mTORC1 as a critical glucose-
250 responsive signaling node that bridges PPP-derived nucleotide metabolism with the
251 maintenance of TFAP2C expression and the expansion of the TE lineage.

252 **Single-cell transcriptomic profiling reveals lineage-specific metabolic signatures**
253 **in bovine blastocysts**

254 To further delineate the metabolic dynamics during bovine preimplantation
255 development and corroborate our in vitro findings, we analyzed single-cell
256 transcriptomic data spanning from the morula to the late blastocyst stages. UMAP
257 dimensionality reduction successfully reconstructed the developmental trajectory and
258 clearly segregated the distinct early embryonic cell lineages, including the TE, ICM, EPI,
259 and PE (Fig. S4A). Heatmap analysis of metabolic gene modules revealed that oxidative
260 phosphorylation (OXPHOS), glycolysis, the HBP, and the PPP exhibit distinct stage- and
261 lineage-specific expression patterns during early embryogenesis (Fig. S4C and Fig 6 A,
262 D, G). To robustly quantify these pathway-level changes and overcome the sparsity of
263 single-cell data, we calculated metabolic module scores, which reflect the overall
264 transcriptional enrichment of these entire metabolic networks within individual cells.

To establish a macroscopic understanding of the metabolic landscape, we first evaluated the comprehensive module scores across all identified developmental stages and cell lineages (Fig. S4B). This overview revealed that OXPHOS maintains a consistently high and relatively stable transcriptional baseline throughout preimplantation development, likely fulfilling the basal energetic demands of the embryo. In contrast, the glucose-driven pathways displayed lower overall absolute scores but exhibited highly dynamic fluctuations, prompting us to further dissect their stage- and lineage-specific variations (Fig. S4B).

We next quantitatively assessed the dynamic shifts in these metabolic modules as embryos progressed through preimplantation development. Bar graphs comparing grouped stages revealed that during the transition from the morula to the mid-blastocyst (MB) stage, the expression modules for both OXPHOS and glycolysis generally increased (Fig. S4D and Fig 6B). However, at the late blastocyst (LB) stage, OXPHOS scores underwent a significant decline, whereas glycolysis continued to sharply rise (Fig. S4D and Fig 6B). This divergent pattern indicates a fundamental metabolic switch in energy production strategies, transitioning toward a predominantly glycolytic state, which is highly consistent with previously reported metabolic shifts in mammalian embryogenesis [21, 29-31].

In contrast to the continuous trajectory of glycolysis, the dynamic changes of the glucose-driven anabolic branches, HBP and PPP, were more complex. The HBP score initially exhibited a transient dip at the early blastocyst (EB) stage before steadily upregulating and peaking at the LB stage (Fig. 6F). Similarly, the PPP module showed a high baseline at the morula stage, followed by a decline at the EB stage, and a subsequent recovery and continuous increase through the MB and LB stages (Fig. 6H). Collectively, these results indicate that glucose-driven metabolic pathways undergo pronounced fluctuations during the morula-to-blastocyst transition.

Importantly, we investigated whether these glucose-driven pathways exhibited lineage-specific partitioning corresponding to our in vitro phenotypes. Quantitative comparison of module scores revealed highly nuanced, pathway-specific metabolic wiring among the cell lineages at the mid- and late-blastocyst stages (Fig. S4B). Notably, the glycolysis scores showed no significant differences between the TE and ICM lineages

296 (Fig. 6C). This finding perfectly aligns with our earlier in vitro observation that inhibiting
297 high-flux glycolysis with YZ9 does not selectively impair TE specification (Fig. S2K, M),
298 confirming that basal glycolysis is broadly utilized rather than acting as a lineage-
299 determining driver.

300 In stark contrast, the HBP module was robustly and specifically enriched in the TE
301 compared to the ICM at the critical mid-blastocyst stage (Fig. 6F). This striking
302 differential expression provides compelling in vivo transcriptomic evidence that HBP
303 activity is preferentially partitioned to the TE, mechanistically explaining why TE
304 specification relies heavily on the HBP-O-GlcNAc-YAP signaling axis.

305 In addition, the PPP module displayed high activity in both embryonic lineages. Notably,
306 the module score in the MB ICM was significantly higher than that in MB TE, whereas LB
307 TE scores were significantly higher than LB PE (Fig. 6I). This dynamic lineage-specific
308 shift suggests that both ICM and TE rely on PPP during blastocyst development, albeit
309 with different temporal requirements. The elevated PPP activity likely reflects the
310 increased demand for nucleotide biosynthesis and redox homeostasis required to
311 sustain rapid cellular proliferation [4, 5, 32, 33]. Consequently, inhibition of PPP is
312 expected to affect both lineages and may therefore produce more severe
313 developmental phenotypes than inhibition of other glucose-derived pathways. This
314 robust and ubiquitous expression pattern perfectly aligns with our in vitro observations:
315 pharmacological suppression of the PPP using 6-AN starting from the zygote stage
316 results in a catastrophic developmental arrest at the morula stage (Fig S1H, I).

317 Discussion

318 In this study, we demonstrate that bovine embryos exhibit a heightened tolerance to
319 glucose deprivation compared to murine models. Although the absence of glucose
320 significantly reduced blastocyst formation rates and compromised overall embryo
321 quality, a subset of embryos retained the capacity to progress beyond the morula stage
322 and successfully cavitate (Fig. 1A, B). This stands in stark contrast to mouse embryos,
323 which undergo irreversible developmental arrest at the morula stage upon glucose
324 withdrawal [2, 5]. In mice, this arrest is primarily attributed to a failure in the glucose-
325 dependent Hippo-YAP axis to regulate CDX2, a factor essential for blastocoel formation

326 in that species [2, 5]. However, while the Hippo pathway–dependent regulation of CDX2
327 is conserved in bovine embryos [23], TE differentiation is not exclusively dependent on
328 the CDX2 regulatory circuit [14, 34]. Consequently, we observed that while glucose
329 deficiency markedly attenuates the Hippo-YAP axis (Fig. 2G–L) and the expression of
330 core TE markers CDX2 and GATA3 (Fig. 2A, B; Fig. S2A, B), bovine embryos remain
331 morphologically capable of cavitation.

332 This phenotypic resilience is also likely underpinned by the superior metabolic flexibility
333 of bovine embryos. Unlike murine embryos, which possess limited endogenous energy
334 stores, bovine embryos are characterized by abundant lipid droplets that serve as
335 alternative energy and biosynthetic substrates during nutrient stress [25, 35, 36].
336 Furthermore, the BO-SOF culture medium utilized in this study provides exogenous
337 pyruvate, lactate, and amino acids, which likely act as a metabolic buffer, sustaining
338 basal development even in the absence of glucose [37-39].

339 Similarly, human embryos exhibit metabolic plasticity and can progress to the
340 blastocyst stage in glucose-deprived conditions [40, 41]. This divergence highlights
341 species-specific metabolic coping strategies and underscores that the bovine model
342 often recapitulates human embryonic development more faithfully than murine
343 models. Therefore, our research model is designed to address the inherent translational
344 limitations of the mouse model.

345 Our findings demonstrate that the three primary branches of glucose metabolism fulfill
346 distinct functional roles during TE differentiation. We observed that basal OCR and
347 exogenous pyruvate uptake remained stable in G− embryos (Fig. 3C–F), and inhibiting
348 glycolytic flux with YZ9 failed to impair blastocyst formation or TE specification (Fig. 1E,
349 F). These results indicate that glucose-derived pyruvate production is redundant for
350 early lineage commitment in bovine embryos. This aligns with isotope tracing studies in
351 mice showing that the carbon contribution of glucose to the pyruvate pool is minimal
352 [5], as well as our metabolomics data showing stable intracellular pyruvate levels in G−
353 blastocysts (Fig. S3A). Collectively, these findings reinforce the conclusion that the
354 requirement for glucose in early embryogenesis is decoupled from bioenergetic
355 production, serving instead to sustain critical biosynthetic flux and metabolic signaling
356 [5, 8, 17].

357 Our results uncover a striking divergence in the requirement for the HBP between
358 bovine and murine embryos. In mice, pharmacological inhibition of either the HBP (via
359 DON) or its downstream effector, OGT (via TT04), triggers a terminal arrest at the morula
360 stage [5]. In contrast, bovine embryos treated with TT04 successfully undergo cavitation
361 despite a significant loss of O-GlcNAcylation (Fig. 3G, H). However, the terminal arrest
362 observed following DON treatment (Fig. S1H, J) indicates that HBP-derived flux remains
363 a fundamental requirement for bovine survival, likely providing substrates for N-glycan
364 synthesis or other vital biosynthetic processes independent of O-GlcNAcylation.

365 Mechanistically, our data suggests a unique relationship between glycosylation and YAP
366 stability. In murine embryos, O-GlcNAc is proposed to stabilize nuclear YAP
367 independent of its phosphorylation status [5, 8, 42]. However, we observed that O-
368 GlcNAc inhibition via TT04 significantly increased p-YAP levels (Fig. 4G, H), while
369 reducing nuclear YAP accumulation and CDX2 expression (Fig. 4A–F). The relationship
370 between glycosylation and YAP phosphorylation during embryogenesis is largely
371 unexplored. However, mutating the Thr241 O-GlcNAc site significantly compromises
372 YAP stability while promoting its phosphorylation in tumor cells [43]. We therefore
373 speculate that inhibition of O-GlcNAc promotes YAP retention in the cytoplasm in
374 bovine embryos, where it becomes increasingly phosphorylated.

375 Interestingly, unlike HBP-specific inhibition, glucose deprivation in bovine embryos
376 resulted in a marked reduction in p-YAP (Fig. 1I, 1J). In cancer cells, AMPK-mediated
377 site-specific phosphorylation serves as a primary mediator of glucose-deficiency
378 signaling [44, 45]. Thus, we speculate that glucose deprivation reduces overall
379 phosphorylation levels, leading to decreased p-YAP.

380 The role of glucose in regulating phosphorylation is further supported by its impact on
381 the mTOR pathway [45]. We found that glucose deprivation significantly decreased
382 phosphorylation of RPS6, a downstream target of mTORC1 (Figure 5A, B). In addition,
383 inhibition of PPP disrupted mTOR signaling, and both PPP inhibition and mTOR
384 suppression markedly reduced the expression of the TE-associated transcription factor
385 TFAP2C (Fig. 5G-K). These findings indicate that PPP activity is essential for maintaining
386 the mTORC1–TFAP2C signaling axis required for proper TE differentiation. Furthermore,
387 inhibition of PPP from the zygote stage resulted in developmental arrest at the morula

stage, which could not be rescued by supplementation with downstream metabolites (Fig. S1H–K). Glucose flux through the PPP serves a critical antioxidant function via NADPH production [32, 33]. When this pathway is disrupted at the G6PD level, murine embryos experience elevated reactive oxygen species (ROS) levels [5, 32]. While uridine can mitigate some defects, full phenotypic restoration requires a combinatorial approach addressing both nucleotide depletion and oxidative stress [5]. We thus speculate that the irreversible arrest observed in bovine embryos is due to elevated ROS levels induced by pathway inhibition, ultimately leading to embryonic lethality.

Beyond direct signaling cascades, glucose availability profoundly shapes the embryonic epigenetic landscape. We observed that disrupted glucose metabolism led to significant reductions in arginine methylation (ADMA and SDMA) alongside a pronounced decrease in the repressive histone modification H3K27me3 (Fig. 3I–N and Fig. S3E–H). Protein arginine methyltransferase 1 (PRMT1) accounts for approximately 85% of ADMA formation in cells [46, 47]. By inhibiting phosphorylation-dependent cytoplasmic retention and proteasomal degradation, PRMT1-mediated methylation promotes YAP stabilization and nuclear accumulation [48]. Therefore, we speculate that glucose may interfere with the Hippo pathway by affecting arginine methylation, thereby influencing TE differentiation. Collectively, our findings highlight a potential link between glucose metabolism and epigenetic control, providing a new avenue for investigating the mechanisms underlying lineage specification.

References

1. M.L. Sutton-McDowall, J.G.T., *Metabolism in the pre-implantation oocyte and embryo*. Animal Reproduction, 2015.
2. Brown, J.J. and D.G. Whittingham, *The roles of pyruvate, lactate and glucose during preimplantation development of embryos from F1 hybrid mice in vitro*. Development, 1991. **112**(1): p. 99-105.
3. Werner, C., T. Doenst, and M. Schwarzer, *Chapter 4 - Metabolic Pathways and Cycles*, in *The Scientist's Guide to Cardiac Metabolism*, M. Schwarzer and T. Doenst, Editors. 2016, Academic Press: Boston. p. 39-55.
4. Stincone, A., et al., *The return of metabolism: biochemistry and physiology of the pentose phosphate pathway*. Biol Rev Camb Philos Soc, 2015. **90**(3): p. 927-63.
5. Chi, F., et al., *Glycolysis-Independent Glucose Metabolism Distinguishes TE from ICM Fate during Mammalian Embryogenesis*. Dev Cell, 2020. **53**(1): p. 9-26 e4.

6. Biggers, J.D., D.G. Whittingham, and R.P. Donahue, *The pattern of energy metabolism in the mouse oöcyte and zygote*. Proceedings of the National Academy of Sciences, 1967. **58**(2): p. 560-567.
7. O'Fallon, J.V. and R.W. Wright, Jr., *Quantitative determination of the pentose phosphate pathway in preimplantation mouse embryos*. Biol Reprod, 1986. **34**(1): p. 58-64.
8. Peng, C., et al., *Regulation of the Hippo-YAP Pathway by Glucose Sensor O-GlcNAcylation*. Molecular Cell, 2017. **68**(3): p. 591-604.e5.
9. Scrivener, A.L., et al., *Protein O-GlcNAcylation in reproductive biology and the impact of metabolic disease*. Human Reproduction Update, 2025. **31**(5): p. 512-531.
10. Düvel, K., et al., *Activation of a Metabolic Gene Regulatory Network Downstream of mTOR Complex 1*. Molecular Cell, 2010. **39**(2): p. 171-183.
11. Simcox, J. and D.W. Lamming, *The central moTOR of metabolism*. Developmental Cell, 2022. **57**(6): p. 691-706.
12. Li, S., et al., *Linker histone H1FOO is required for bovine preimplantation development by regulating lineage specification and chromatin structuredagger*. Biol Reprod, 2022. **107**(6): p. 1425-1438.
13. Dang, Y., et al., *The lysine deacetylase activity of histone deacetylases 1 and 2 is required to safeguard zygotic genome activation in mice and cattle*. Development, 2022. **149**(11).
14. Shi, Y., et al., *Functional role of GATA3 and CDX2 in lineage specification during bovine early embryonic development*. Reproduction, 2023.
15. Guerif, F., et al., *A simple approach for COnsumption and RElease (CORE) analysis of metabolic activity in single mammalian embryos*. PLoS One, 2013. **8**(8): p. e67834.
16. Muller, B., et al., *Application of extracellular flux analysis for determining mitochondrial function in mammalian oocytes and early embryos*. Scientific Reports, 2019. **9**(1): p. 16778.
17. Cao, D., et al., *Selective utilization of glucose metabolism guides mammalian gastrulation*. Nature, 2024. **634**(8035): p. 919-928.
18. Wu, X., et al., *TEAD4 regulates KRT8 and YAP in preimplantation embryos in mice but not in cattle*. Reproduction, 2024. **167**(3).
19. Li, S., et al., *NOTCH signaling pathway is required for bovine early embryonic developmentdagger*. Biol Reprod, 2021. **105**(2): p. 332-344.
20. Hu, B., et al., *Single-cell RNA-Seq reveals the earliest lineage specification and X chromosome dosage compensation in bovine preimplantation embryos*. FASEB J, 2024. **38**(4): p. e23492.
21. Malkowska, A., et al., *A hexa-species transcriptome atlas of mammalian embryogenesis delineates metabolic regulation across three different implantation modes*. Nature Communications, 2022. **13**(1).
22. Wu, Z. and K.-L. Guan, *Hippo Signaling in Embryogenesis and Development*. Trends in Biochemical Sciences, 2021. **46**(1): p. 51-63.
23. Gerri, C., et al., *A conserved role of the Hippo signalling pathway in initiation of the first lineage specification event across mammals*. Development, 2023. **150**(8).
24. Uhde, K., et al., *Exposure to elevated glucose concentrations alters the metabolomic profile of bovine blastocysts*. PLOS ONE, 2018. **13**(6): p. e0199310.

25. Herrick, J.R., et al., *Developmental and molecular response of bovine embryos to reduced nutrients in vitro*. Reproduction and Fertility, 2020. **1**(1): p. 51-65.
26. Krisher, R.L. and J.R. Herrick, *Bovine embryo production in vitro: evolution of culture media and commercial perspectives*. Anim Reprod, 2024. **21**(3): p. e20240051.
27. Pladevall-Morera, D. and J.J. Zylicz, *Chromatin as a sensor of metabolic changes during early development*. Front Cell Dev Biol, 2022. **10**: p. 1014498.
28. Ma, C., et al., *mTOR hypoactivity leads to trophectoderm cell failure by enhancing lysosomal activation and disrupting the cytoskeleton in preimplantation embryo*. Cell Biosci, 2023. **13**(1): p. 219.
29. Thompson, J.G., et al., *Oxygen uptake and carbohydrate metabolism by in vitro derived bovine embryos*. J Reprod Fertil, 1996. **106**(2): p. 299-306.
30. Banliat, C., et al., *The proteomic analysis of bovine embryos developed in vivo or in vitro reveals the contribution of the maternal environment to early embryo*. BMC Genomics, 2022. **23**(1): p. 839.
31. Traut, M., et al., *Deregulation of oxidative phosphorylation pathways in embryos derived in vitro from prepubertal and pubertal heifers based on whole-transcriptome sequencing*. BMC Genomics, 2024. **25**(1): p. 632.
32. Warzych, E., P. Lipinska, and E. Sell-Kubiak, *Pentose phosphate pathway inhibition during in vitro maturation substantially affects the metabolism of bovine COCs and blastocysts*. Theriogenology, 2024. **230**: p. 72-80.
33. Braga, J.V., et al., *The role of the pentose phosphate pathway on reproductive functions*. Anim Reprod, 2025. **22**(4): p. e20240130.
34. Goissis, M.D. and J.B. Cibelli, *Functional characterization of CDX2 during bovine preimplantation development in vitro*. Molecular Reproduction and Development, 2014. **81**(10): p. 962-970.
35. Barceló-Fimbres, M. and G.E. Seidel, *Cross-validation of techniques for measuring lipid content of bovine oocytes and blastocysts*. Theriogenology, 2011. **75**(3): p. 434-444.
36. Kajdasz, A., et al., *Lipid Stores and Lipid Metabolism Associated Gene Expression in Porcine and Bovine Parthenogenetic Embryos Revealed by Fluorescent Staining and RNA-seq*. Int J Mol Sci, 2020. **21**(18).
37. Pasquariello, R., et al., *Lipid Enriched Reduced Nutrient Culture Medium Improves Bovine Blastocyst Formation*. Reprod Fertil, 2023. **4**(4).
38. Sudano, M.J., et al., *Lipid content and apoptosis of in vitro-produced bovine embryos as determinants of susceptibility to vitrification*. Theriogenology, 2011. **75**(7): p. 1211-1220.
39. Ordoñez-Leon, E.A., et al., *Lipid droplet analysis using in vitro bovine oocytes and embryos*. Reprod Domest Anim, 2014. **49**(2): p. 306-14.
40. Coates, A., et al., *Glucose-free medium in human in vitro fertilization and embryo transfer: a large-scale, prospective, randomized clinical trial*. Fertility and Sterility, 1999. **72**(2): p. 229-232.
41. Conaghan, J., et al., *Effects of pyruvate and glucose on the development of human preimplantation embryos in vitro*. Journal of Reproduction and Fertility, 1993. **99**(1): p. 87-95.
42. Lei, Y., et al., *Protein O-GlcNAcylation coupled to Hippo signaling drives vascular dysfunction in diabetic retinopathy*. Nat Commun, 2024. **15**(1): p. 9334.

43. Zhang, X., et al., *The essential role of YAP O-GlcNAcylation in high-glucose-stimulated liver tumorigenesis*. Nature Communications, 2017. **8**(1): p. 15280.
44. Mo, J.S., et al., *Cellular energy stress induces AMPK-mediated regulation of YAP and the Hippo pathway*. Nat Cell Biol, 2015. **17**(4): p. 500-10.
45. Santo-Domingo, J., et al., *Glucose-dependent phosphorylation signaling pathways and crosstalk to mitochondrial respiration in insulin secreting cells*. Cell Communication and Signaling, 2019. **17**(1): p. 14.
46. Bedford, M.T. and S.G. Clarke, *Protein Arginine Methylation in Mammals: Who, What, and Why*. Molecular Cell, 2009. **33**(1): p. 1-13.
47. Di Lorenzo, A. and M.T. Bedford, *Histone arginine methylation*. FEBS Letters, 2011. **585**(13): p. 2024-2031.
48. Hong, X.-L., et al., *Positive feedback between arginine methylation of YAP and methionine transporter SLC43A2 drives anticancer drug resistance*. Nature Communications, 2025. **16**(1): p. 87.

Acknowledgements

We thank Prof. Henry J Leese for his helpful discussion.

Competing interests

The authors declare no competing or financial interests.

Author contributions

J.Q. conceived the project, designed and performed all experiments, analysed and interpreted the data, and drafted and critically revised the manuscript. R.S. secured funding for the project and critically revised the manuscript.

Funding

There were no project specific funds for this work. Reagents used in this study were provided by the R.S. laboratory through general laboratory funds.

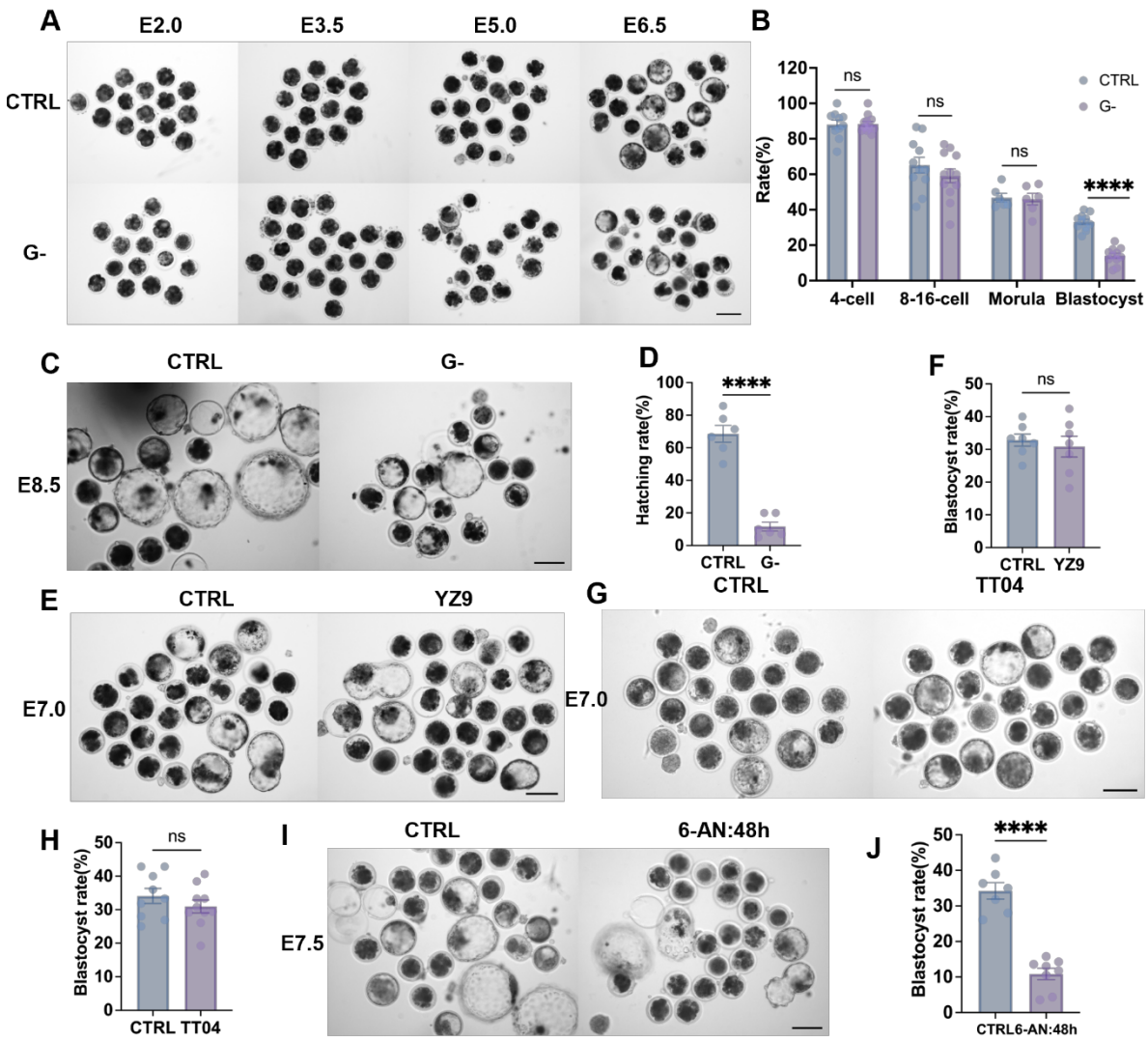

Fig 1 Glucose deprivation and inhibition of glucose metabolism impair bovine blastocyst formation.

(A–D) Representative brightfield images of bovine embryos cultured in G− or CTRL media. Quantification of the proportion of embryos developing to the 4-cell (E2.0), 8–16-cell (E3.5), morula (E5.0) and blastocyst (E6.5) stages, and the proportion of hatching embryos at E8.5.

(E, F) Representative images and corresponding blastocyst formation rates of E7.0 embryos cultured in the presence of the glycolysis inhibitor YZ9, relative to CTRL.

(G, H) Representative images and blastocyst formation rates of E7.0 embryos cultured with the HBP inhibitor TT04, relative to CTRL.

(I, J) Representative images and blastocyst formation rates of E7.5 embryos cultured with the PPP inhibitor 6-AN for 48 hours, relative to CTRL.

All percentages were calculated relative to the total number of zygotes cultured per treatment. Data are presented as mean ± SEM from at least six independent replicates (≥15 embryos per group). Statistical significance was determined using a two-tailed unpaired Student's t-test: ns, not significant; **P < 0.01; ****P < 0.0001. Scale bars, 50 μm.

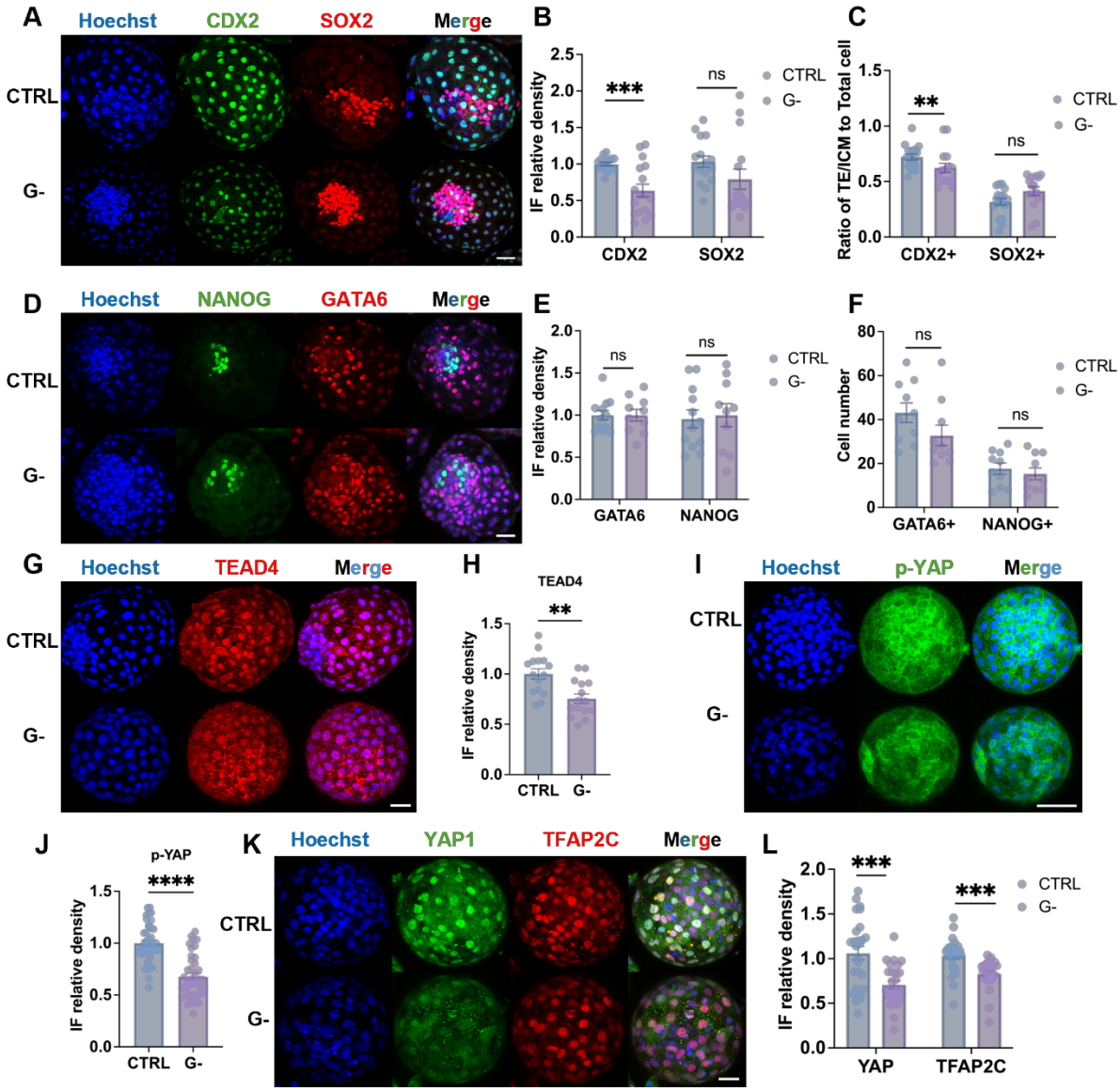

Fig 2 Glucose deprivation attenuates the Hippo signaling to impair TE specification

(A–C) Immunofluorescence staining and quantitative analysis of the TE marker CDX2 and ICM marker SOX2 in E7.0 bovine blastocysts cultured under CTRL and G− conditions.

(D–F) Immunofluorescence staining and quantification of EPI marker NANOG and PrE marker GATA6 in E8.5 blastocysts cultured under CTRL and G− conditions.

565 (G–L) Immunofluorescence staining and quantitative analysis of Hippo pathway components,
566 including TEAD4 (G, H), p-YAP (I, J), YAP (K, L), and TFAP2C (K, L), in E7.0 blastocysts cultured under
567 CTRL and G− conditions.

568 For quantification, relative lineage-specific cell ratios were calculated for TE (CDX2$^+$/Hoechst$^+$), ICM
569 (SOX2$^+$/Hoechst$^+$), EPI (NANOG$^+$/Hoechst$^+$), and PrE (GATA6$^+$/Hoechst$^+$) populations (n ≥ 3
570 biological replicates, with ≥3 blastocysts per group). Data are presented as mean ± SEM. Statistical
571 significance was determined using a two-tailed unpaired Student's t-test: ns, not significant; **P <
572 0.01; ***P < 0.001; ****P < 0.0001. Scale bars, 100 μm.

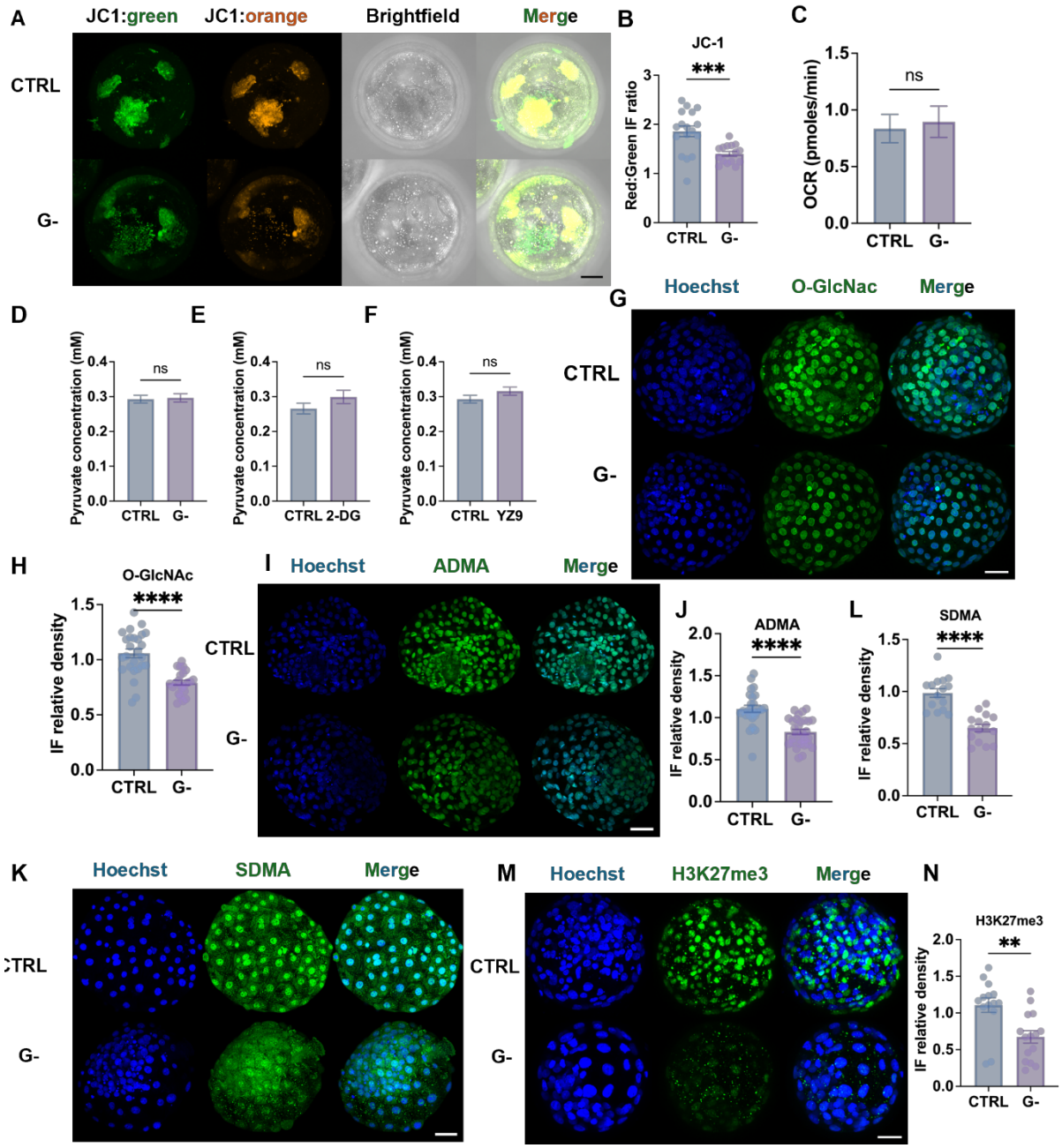

573

Fig 3 Glucose deprivation compromises mitochondrial function and epigenetic landscapes

(A, B) Representative fluorescence images of JC-1 staining in CTRL and G− blastocysts. Orange fluorescence indicates J-aggregates, whereas green fluorescence indicates J-monomers. Quantification of the red/green JC-1 fluorescence ratio.

(C) OCR measured by Seahorse XF analysis in CTRL and G− blastocysts.

(D–F) Pyruvate concentrations in culture medium following 24 h embryo culture under G−, 2-DG-treated, and YZ9-treated conditions, relative to CTRL.

(G, H) Representative immunofluorescence images and corresponding quantification of global O-GlcNAc (green) levels in CTRL and G− blastocysts.

(I-N) Representative immunofluorescence images and quantification of ADMA, SDMA, H3K27me3 in CTRL and G− blastocysts.

Data are presented as mean ± SEM. Statistical significance was determined using a two-tailed unpaired Student's t-test (n ≥ 3 biological replicates, with ≥5 blastocysts per group): ns, not significant; **P < 0.01; ***P < 0.001; ****P < 0.0001. Scale bars, 100 μm.

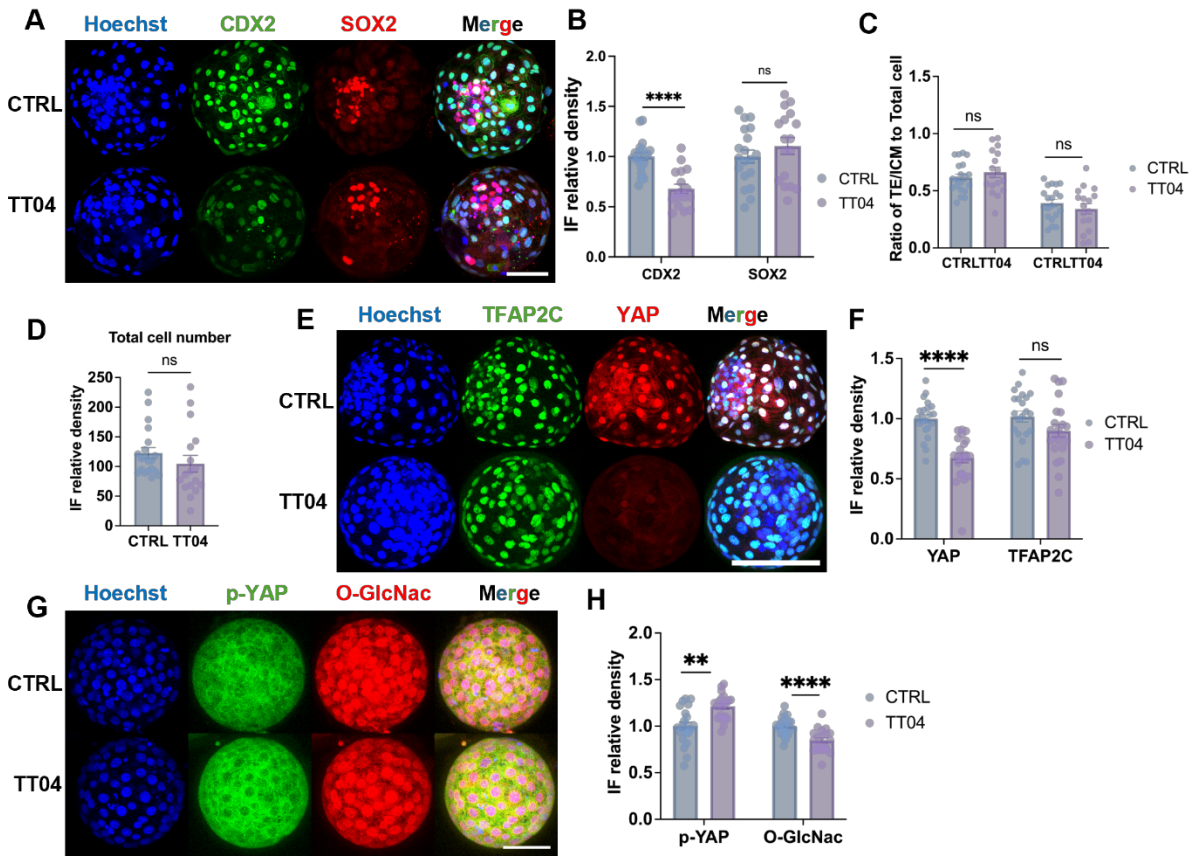

590 **Fig 4 Inhibition of O-GlcNAc disrupts YAP and TE specification**

591 (A, B) Representative immunofluorescence images and quantitative analysis of CDX2 and SOX2 in
592 E7.0 embryos cultured under CTRL and TT04 treated conditions.

593 (C, D) Quantitative analysis of total cell number (Hoechst$^+$), and the proportions of TE
594 (CDX2$^+$/Hoechst$^+$) and ICM (SOX2$^+$/Hoechst$^+$) cells in E7.0 embryos cultured under CTRL and TT04-
595 treated conditions.

596 (E, F) Representative immunofluorescence images and quantitative analysis of YAP and TFAP2C in
597 E7.0 embryos cultured CTRL and TT04 treated conditions.

598 (G, H) Representative immunofluorescence images and quantitative analysis of p-YAP and global O-
599 GlcNAc in E7.0 embryos cultured CTRL and TT04-treated conditions.

600 Data are presented as mean ± SEM. n≥3 independent biological replicates, with ≥5 blastocysts per
601 group. Statistical significance was determined using a two-tailed unpaired Student's t-test. ns, not
602 significant; **P < 0.01; ****P < 0.0001. Scale bars, 100 μm.

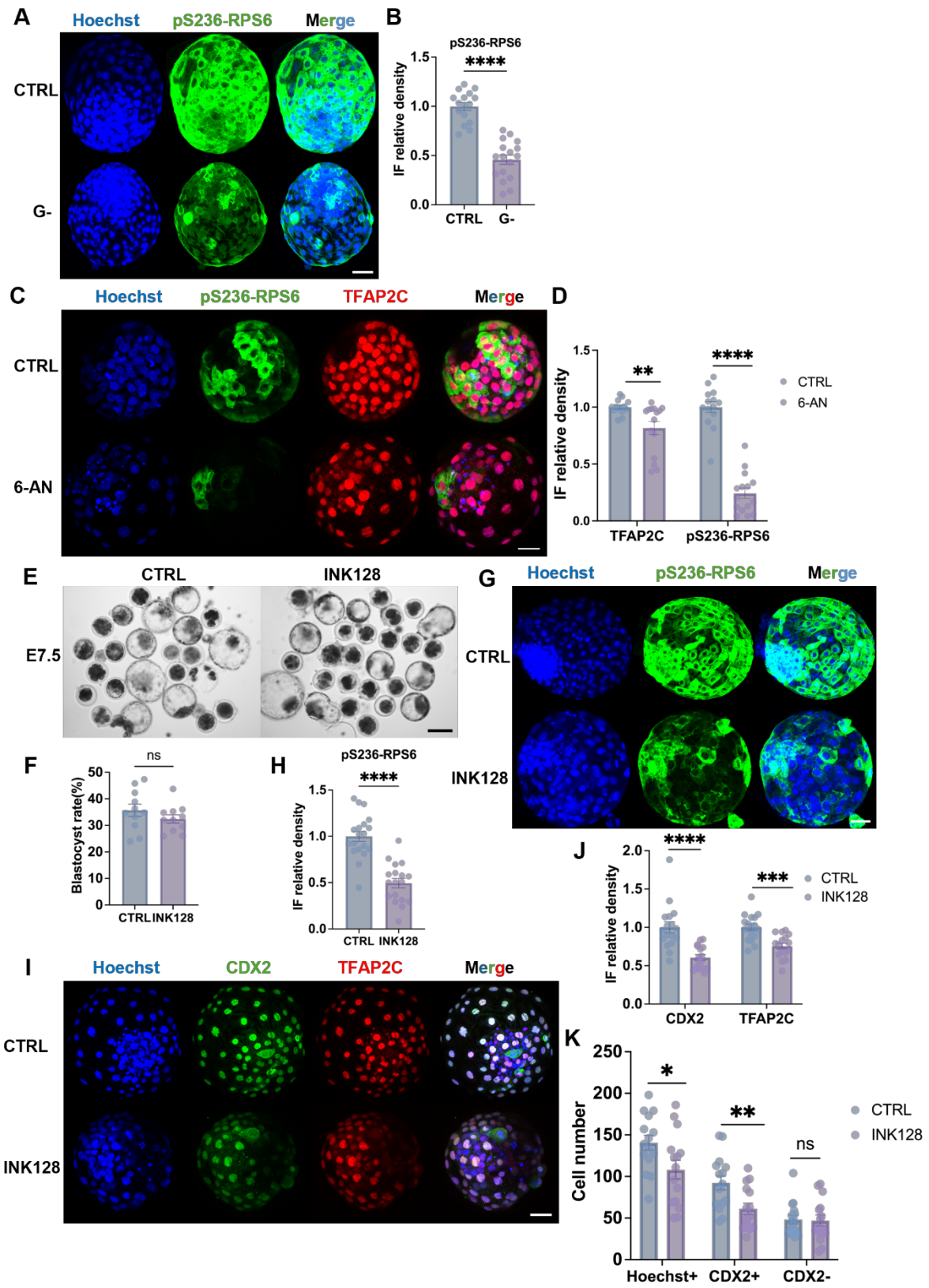

603

604 **Fig 5 Inhibition of the PPP suppresses mTOR activity and disrupts TE differentiation**

605 (A, B) Representative immunofluorescence images and quantitative analysis of pS236-RPS6 in E7.0
606 embryos cultured under CTRL or G– conditions.

607 (C, D) Representative immunofluorescence images and quantitative analysis of pS236-RPS6 and
608 TFAP2C in E7.5 embryos cultured under CTRL or 6-AN-treated conditions.

609 (E, F) Representative bright-field images and quantification of blastocyst formation rates in E7.0
610 embryos cultured under CTRL or INK128-treated conditions. Scale bar, 50 μm.

611 (G, H) Representative immunofluorescence images and quantitative analysis of pS236-RPS6 in E7.5
612 embryos cultured under CTRL or INK128-treated conditions.

613 (I–K) Representative immunofluorescence images and quantitative analysis of CDX2 and TFAP2C in
614 embryos under CTRL or INK128-treated conditions.

615 Data are presented as mean ± SEM. n ≥3 independent biological replicates, with ≥5 embryos per
616 groups. Statistical significance was determined using a two-tailed unpaired Student's t-test: ns, not
617 significant; *P < 0.05; **P < 0.01; ***P < 0.001; ****P < 0.0001. Scale bar, 100 μm

618

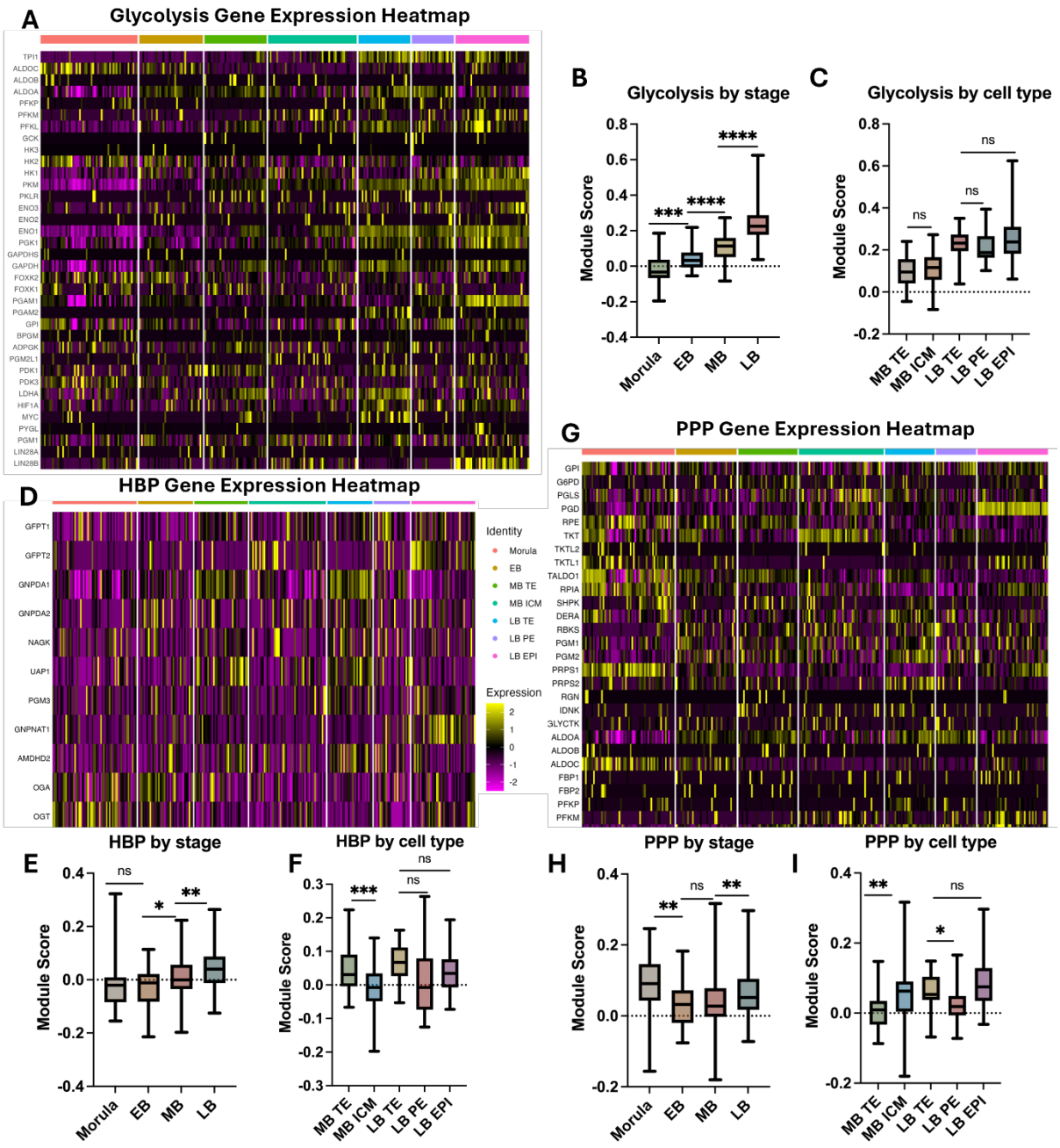

Fig 6 Quantitative analysis of metabolic pathway module scores during bovine preimplantation development.

(A, D, G) Heatmap showing the expression of glycolysis,HBP and PPP module genes.

(B, E, H) Bar graphs comparing the dynamic changes in module scores of glycolysis, HBP and PPP across grouped developmental stages.

(C, F, I) Bar graphs illustrating the differences in module scores among TE, ICM, PE and EPI at the mid- and late-blastocyst stages.

Data are presented as mean ± SEM. Statistical significance was determined using Welch's one-way ANOVA, followed by Dunnett's T3 post-hoc test: ns, not significant; *P < 0.05; **P < 0.01; ***P < 0.001; ****P < 0.0001.